Granitic Rock Weathering and Clay Deposit Formation at the Al Barzah Area, Westcentral Arabian Shield, Saudi Arabia

Rami A. Bakhsh
Mineral Resources and Rocks Department, Faculty of Earth Sciences, King Abdulaziz University, Jeddah, Saudi Arabia
rbakhsh@kau.edu.sa (corresponding author)

Received: 17 November 2025 | Revised: 7 January 2026 and 30 January 2026 | Accepted: 7 February 2026

 DOI: https://doi.org/10.48084/etasr.16315

ABSTRACT

The present study investigates the progressive steps of the alteration and destruction of primary minerals and related textures in granitic rocks in the Al Barzah area during weathering processes. The study area is located in the west-central part of Saudi Arabia and represents a low, cultivated, closed area within the Arabian Shield. Geologically, the area includes Neoproterozoic weathered granite rocks, which are unconformably overlain by Tertiary red clays and sandstones of the Haddat Asham Formation, black basaltic volcanics, and Quaternary wadi deposits. The weathering processes of the studied granitic rocks involve the initial transformation of feldspar, biotite, hornblende, and quartz in the parent granitic rocks into kaolinized feldspar, chloritized hornblende, and hematitized biotite, respectively. As weathering progresses, the transformed minerals become highly obliterated, and newly formed secondary clay minerals mixed with iron oxide appear. This is accompanied by the complete destruction of the original crystalline textures. The clay deposits formed a characteristic white horizon below the Tertiary red clastics and overlying black basalts.

Keywords-Saudi Arabia; Arabian shield rocks; weathering of granitic rocks

I. INTRODUCTION

A. Aims of the Study

The Al Barzah area is a distinctive depression in the Arabian Shield rocks, as shown in Figure 1. It is located about 150 km northeast of the city of Jeddah within the Makkah district. The origin and mechanism of formation of this depression are lithologically and structurally controlled. This is confirmed by the presence of many wide areas (wadies) running in northwestern and northeastern directions. The present study aims to provide a detailed analysis of the petrographic and mineralogical evolution of the weathering of the granitic rocks in the study area, using field and laboratory work to understand the stages of weathering processes and the resulting mineral phases.

B. Sampling and Methods of Study

This field-based study involves delineating and sampling the different horizons of weathering profiles in horizontal and lateral directions. Samples are collected systematically from one profile, beginning with the parent granitic rocks and progressing through slightly, moderately, and highly weathered granites, as depicted in Figure 2. The samples are then described petrographically and analyzed geochemically. The geochemical composition of the whole-rock samples was analyzed at ALS Arabia in Jeddah, Saudi Arabia. Major element oxides were quantified using X-ray fluorescence. Loss on Ignition (LOI) was determined as part of the X-ray Fluorescence (XRF) preparation via the WST-SEQ standard. X-ray Diffraction (XRD) analyses were carried out on six samples representing the parent granitic rocks and the overlying weathering horizons. The XRD results are shown alongside the weathering profile section. Global Mapper and ArcGIS software were used to prepare satellite images and geological maps of the study area, utilizing CorelDraw to draw the different weathering horizons and present the mineralogical evolution of the studied weathering profile.

C. Geologic Setting

The geology of the Makkah area includes the Arabian Shield (Neoproterozoic) with igneous and metamorphic rocks such as gabbro, granite, and diorite, as well as metamorphic rocks, such as schist and amphibolite, and tertiary sedimentary and volcanic rocks [1, 2]. The Arabian Shield rocks in the Makkah district were also analyzed [3], concluding that these rocks are composed of the Makkah Suite intrusive rocks (gabbros, diorites, and granites of Tonian age, ~1000 m.y.) and the layered Jeddah Group rocks. The Tertiary succession is exhibited in the Haddat Asham formations and the overlying basic volcanics (Harrat). This succession and the overlying basic volcanics are equivalent to those described in the Usfan area [4]. The area contains a shallow groundwater aquifer within Quaternary wadi deposits.

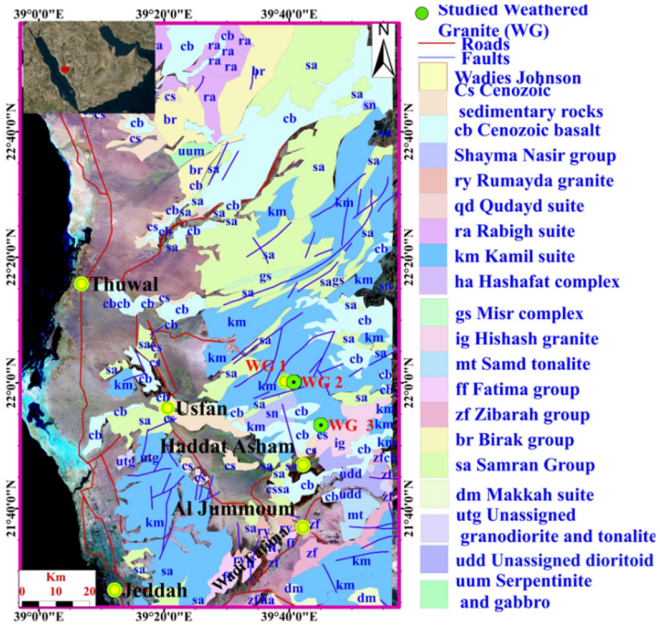

Fig. 1. Geologic map of Makkah district (Johnson, 2006) showing the location of the studied weathering profile of Al Barzah area.

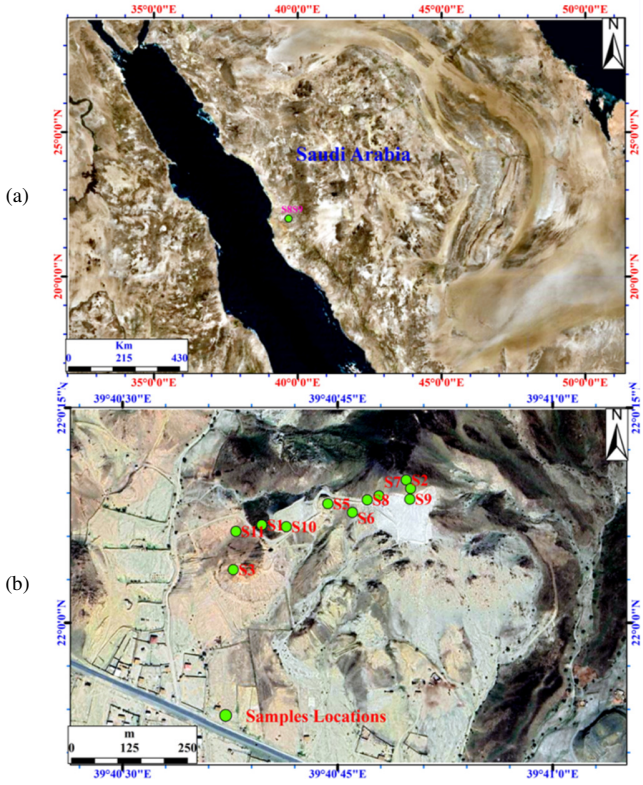

Fig. 2. (a) General location of Al Barzah area, (b) locations of the samples studied.

II. FIELD, MEG-AND MICROSCOPIC DESCRIPTION OF THE WEATHERING PROFILE

The pink granite rocks and white weathering products (clay deposits) that were studied are currently found in the Al Barzah depression and along the highway from Haddat Asham to Al Barzah. The white weathering products are shiny and range in thickness from 8 m to 15 m, as shown in Figures 3 and 4. There is a characteristic gradation from yellowish-brown, slightly weathered rocks to white, kaolinitic, highly weathered rocks. Along the Haddat Asham–Al Barzah highway, the weathered granitic rocks are only represented by the topmost, highly weathered parts, and the parent and slightly to highly weathered rocks are unexposed, as presented in Figure 5.

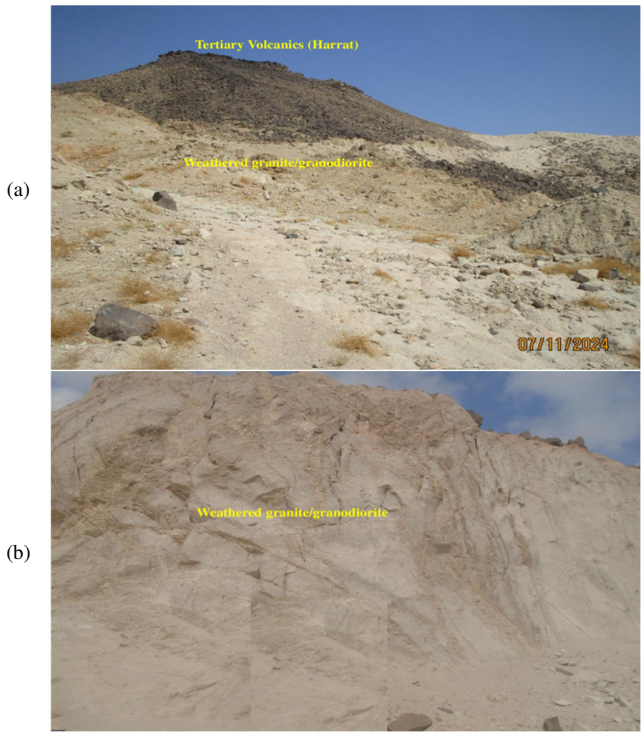

Fig. 3. Field photos of the different horizons of the studied weathering profile in Al Barzah area: (a) tertiary volcanic rocks, (b) granitic rocks.

The current field descriptions and measurements revealed different weathering horizons in the topmost white, highly weathered kaolinitic granites derived from the parental granitic rocks, as displayed in Figure 6. The progressive weathering of these granites formed thick horizons (up to 14 m) above unweathered granite, in which the original parent rock's preexisting structures are preserved. Similar horizons are described as "lithomerge" in the French literature and as a "saprolite" in the English literature [5]. The saprolite horizon is uneven and can be subdivided into four successive zones that always occur in the same order. The contacts between these horizons are often gradational. XRD analyses revealed a general decrease in the peaks or disappearance of the primary mineral constituents of granite, i.e., quartz, orthoclase, microcline, and albite, followed by the appearance of peaks of clay minerals, e.g., kaolinite, illite, and smectite. The source rocks are clearly exposed on the slope of the main wadis in the Al Barzah area. This unit is composed of fresh to partially weathered, massive, medium-to-coarse-grained, pink rocks that are highly jointed, as shown in Figure 7. Kaolinization and the accumulation of residual debris are common along joints and

fractures. The slightly weathered granite consists of angular blocks interlocked with a kaolinitic matrix. Spheroidal scaling is also common. Toward the upper part of this zone, the granite blocks gradually disintegrate and become displaced, and the small granitic fragments become highly kaolinized. The progressively altered rock in the middle part of Figure 6 is a mixture of highly decomposed granite. In its lower part, it contains irregularly distributed rounded to subrounded core stones and quartz grains embedded in a kaolin-rich matrix. The weathering products of this zone retain the original joint structures of the parent granite. The topmost, highly weathered horizon is light gray to white with brown and red shades, representing the ultimate weathering products of the parent granite, and merges downward into the underlying zones. This horizon is directly overlain by the red clastic succession of the Haddat Asham Formation and the overlying black basaltic lava flows (harrat).

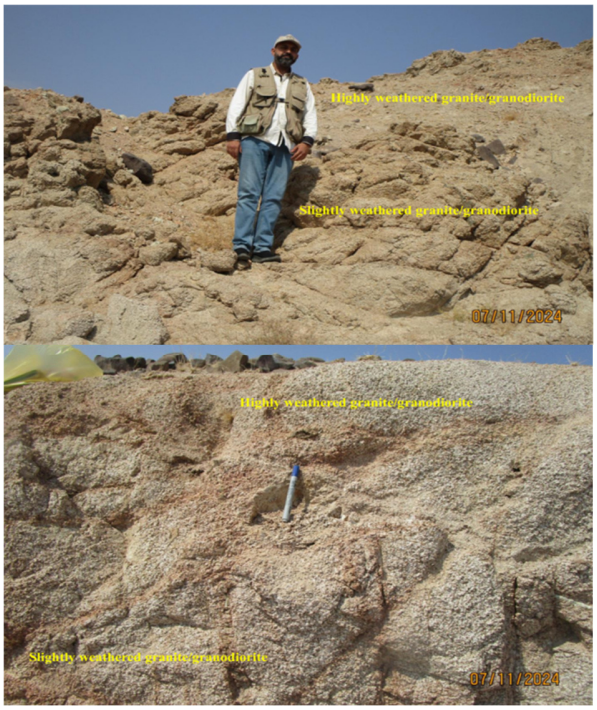

Fig. 4. Detailed field photos of the different horizons of the studied weathering profile in Al Barzah area.

A. Microscopic Description of the Parental Granitic Rocks

The granitic rocks are rich in green hornblende and biotite. Representative fresh samples are used for microscopic descriptions and bulk geochemical analyses, as portrayed in Figures 8 and 9. The partially weathered rock horizon consists entirely of equigranular crystals of sodium plagioclase, orthoclase, microcline, biotite, and muscovite, with less predominant green hornblende. The slightly to highly weathered samples consist of friable, white, kaolinized feldspar crystals intermixed with a friable clay matrix, containing less frequent, stained, altered hornblende and biotite lathes, as presented in Figures 9 (c) and (d). Microscopically, the parental granitic rocks reveal their holocrystalline and phaneritic textural features. Thin sections under plain polarized light show an abundance of felsic minerals compared to mafic minerals. Fresh parent granites consist of feldspar, quartz, and a small amount of mafic minerals (hornblende, biotite, and muscovite) with a well-developed hypidiomorphic granitic texture.

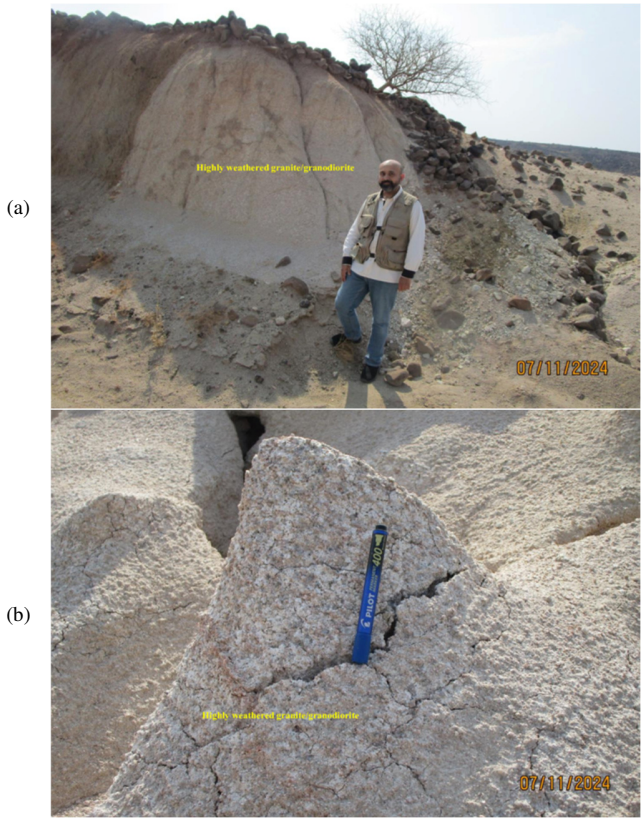

Fig. 5. Detailed field photos of the different horizons of the studied weathering profile in Al Barzah area.

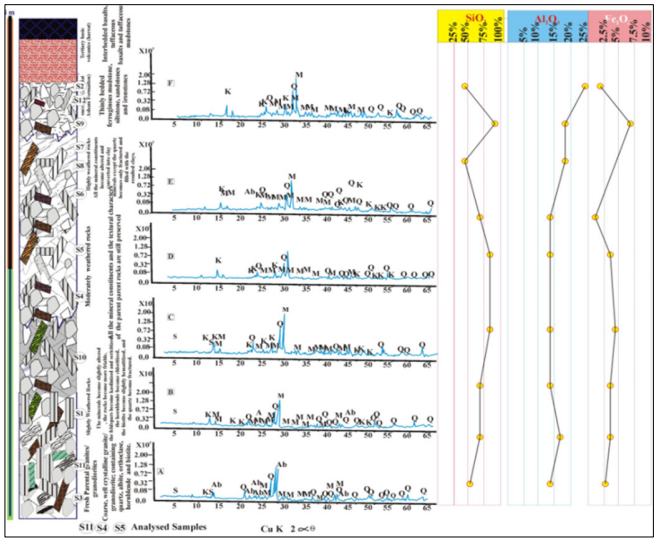

Fig. 6. Detailed stratigraphic section showing the different horizons of the studied weathering profile (from base to top) in Al Barzah area XRD patterns of the different horizons of the weathering profile: S=Smectite, K= kaolinite, Ab= Albite, I= Illite, M= Microcline, q= quartz.

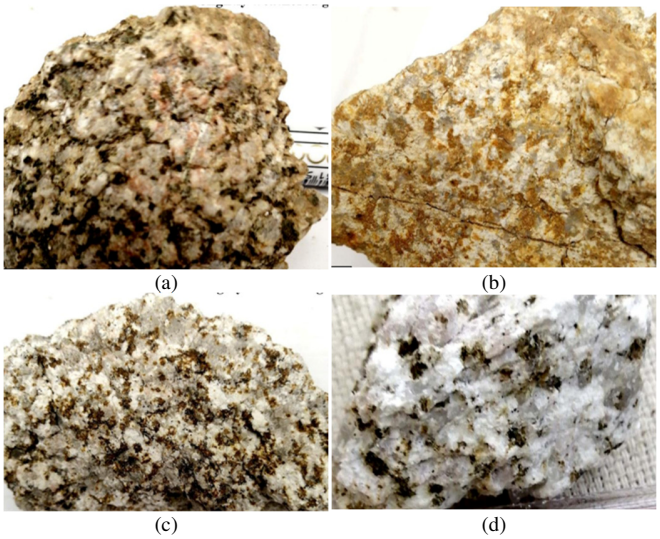

Fig. 7. Hand samples of the different horizons of the studied weathering profile in Al Barzah area: (a), (b): parent granitic rocks slightly weathered; (c), (d): highly weathered granite.

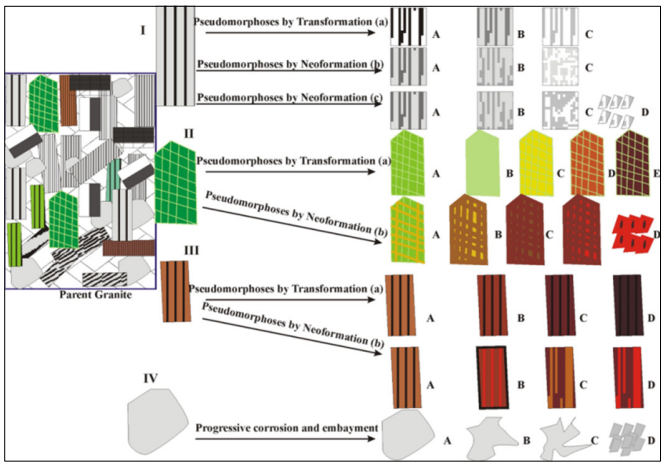

Fig. 8. Petrographic evolution of the different mineral phases of the studied weathering profile in Al Barzah area.

B. *Mineralogic Evolution and Alteration of Different Minerals*

In slightly to highly weathered granite, quartz, potash, and plagioclase feldspars are the least altered minerals. Meanwhile, hornblende becomes slightly chloritized, and muscovite and biotite become partially kaolinized.

1) *Feldspars*

K-feldspars: Potash feldspars, such as microcline and orthoclase, are much more stable than the associated plagioclase feldspars in different weathering zones. Although they are not easily altered into new minerals, they are commonly embayed and corroded (Figure 8I(a)). Relics of potash feldspar crystals are sporadically distributed within the kaolinite-rich matrix of the argillaceous zone. Alteration into kaolinite is prevalent along the twinning and cleavage planes. During the alteration, sericite and illite appear to form instead of potash feldspar crystals.

2) *Plagioclase Feldspars*

Plagioclase feldspars exhibit lamellar twinning in their crystals (primarily albite) and have undergone extensive alteration and obliteration into dusty minerals composed of a mixture of kaolinite and sericite. In slightly weathered granite, alteration processes begin with the relatively irregular obliteration of plagioclase crystals, resulting in the formation of clayey surface layers containing minute sericite crystals, as shown in Figures 10 (a-d). In other cases, the alteration is more regular, commonly occurring along twinning planes and resulting in commonly oriented sericite patches along these planes, as illustrated in Figures 10 (e) and 10 (f). In slightly to highly weathered granites, plagioclase crystals appear to be fully digested, leaving only sporadic pseudomorphs, commonly filled with sericite, in association with kaolinite, as displayed in Figures 10 (g) and 10 (h).

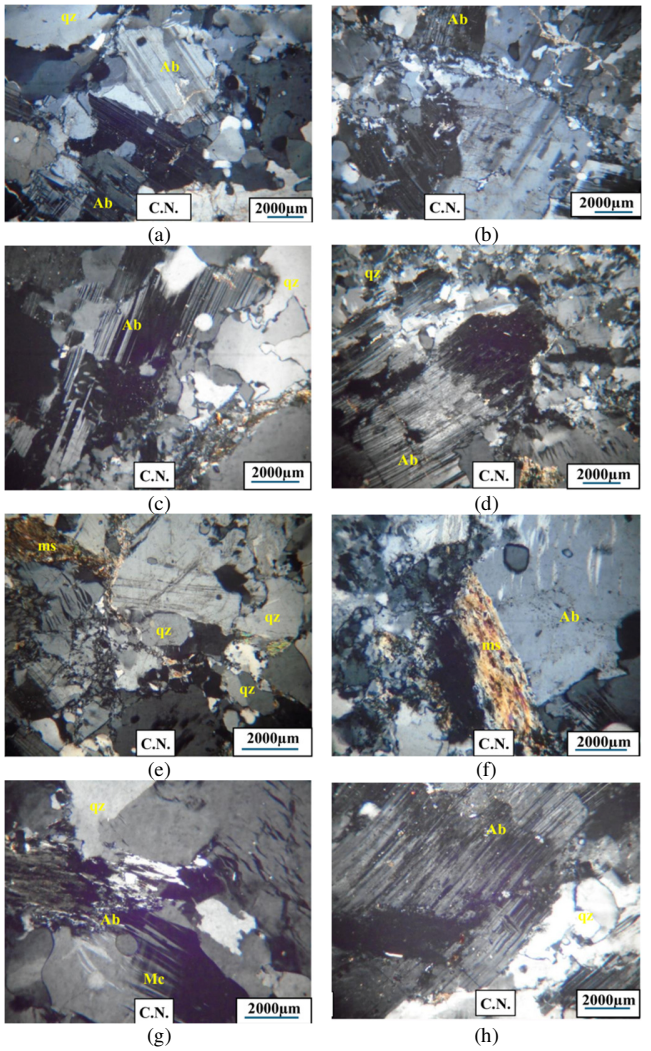

Fig. 9. Petrographic description of the parental granitic rocks of the studied weathering profile in Al Barzah area: (a), (b), (c), (d): hypidiomorphic granitic texture, (e), (f): oriented sericite patches, (g), (h): sericite, in association with kaolinite. Ab:albite, Qz:quartz, Ms:muscovite, Mc:microcline, O.L.:ordinary light, C.N.:crossed nicols.

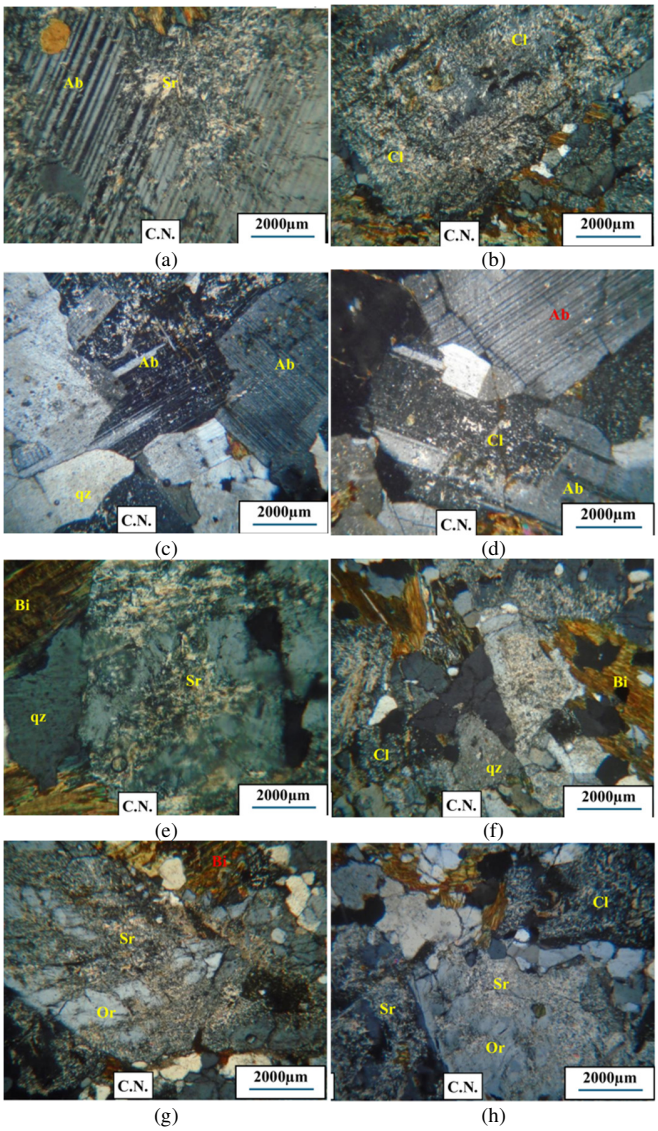

Fig. 10. Petrographic description of the kaolinization stages of the feldspars of the studied weathering profile in Al Barzah area: (a), (b), (c), (d): layers containing minute sericite crystals, (e), (f): oriented sericite patches, (g), (h): sericite, in association with kaolinite. Ab: albite, Or: orthoclase, Qz: quartz, Sr: sericite, Bi: biotite, Cl: clay minerals.

3) Hornblende

Hornblende crystals (Figure 8III) are generally preserved in slightly weathered granite. In the middle and upper parts of the weathering profiles, two main types of alteration are observed:

- Pseudomorphs by transformation as a result of homogenization and chloritization, which led to the formation of large chlorite crystals and aggregates that pseudomorph the original hornblende crystals [6], as shown in Figures 8II(a) and 11 (a-d). The formed chlorite flakes are oxidized and pseudomorphosed by reddish-yellow and brown hematite flakes (Figures 8 II(a) and 12 (e-f)).
- Pseudomorphs by neomorphism, where hornblende crystals progressively exfoliate and hematite forms along two sets of cleavage planes (Figures 8II(b), 11 (a-b)). The ultimate stage of hematitization leads to the formation of parallel laminae of hematite and interstratified vermiculite, as presented in Figures 8II(b), 11 (c-f), and 13 (a-d). Authors in [11] described a similar stage of chloritization and hematitization of hornblende and resulting chlorites, in Turonian laterites along Nubian Shield rocks and the overlying Cretaceous succession in the Gabal El Dawi area on the Quseir-Qena road in the Eastern Desert of Egypt.

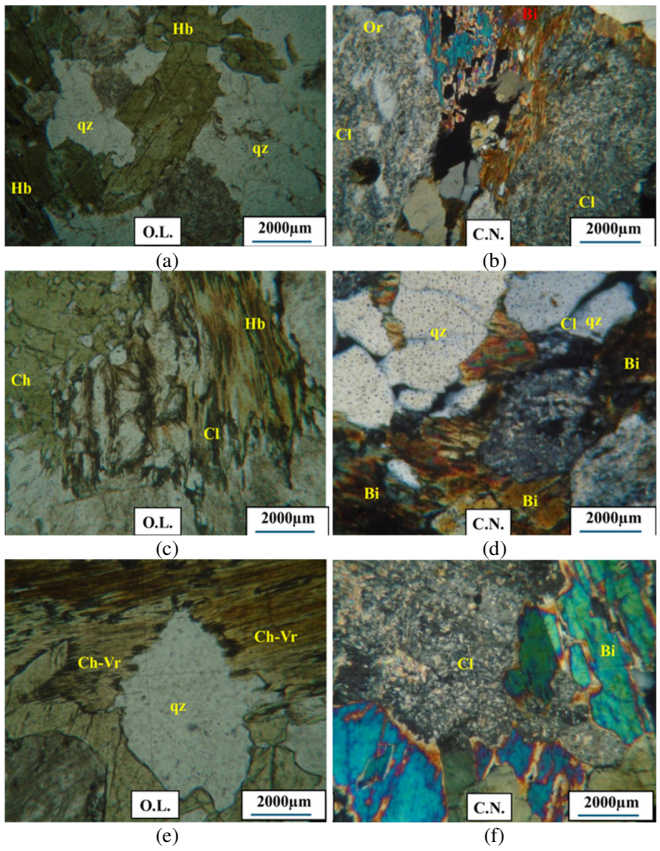

Fig. 11. Petrographic description of the chloritization of the hornblende of the studied weathering profile in Al Barzah area: (a), (b), (c), (d): large chlorite crystals and aggregates that pseudomorph the original hornblende crystals, (e), (f): parallel laminae of hematite and interstratified vermiculite. Qz: quartz, Hb: hornblende, Cl: clay minerals, Ch-Vr: chlorite-vermiculite, bi: biotite.

4) Biotite

The biotite crystals in the lower, fresh-to-slightly-weathered rocks still exhibit their original euhedral-to-subhedral habit. The mottled appearance of the moderately to highly weathered zone appears to result from the progressive alteration of the original brown biotite crystals and the formation of lighter pseudomorphs of highly altered biotite (Figure 8III(a)). Further alteration leads to the formation of intergrade vermiculite-chlorite, accompanied by the gradual separation of small, reddish-brown, pseudohexagonal iron oxyhydroxide flakes and blotches, as shown in Figures 8III(b) and 13 (e-f). Authors in [7, 8] discussed the alteration and obliteration of biotite during weathering and the formation of red beds.

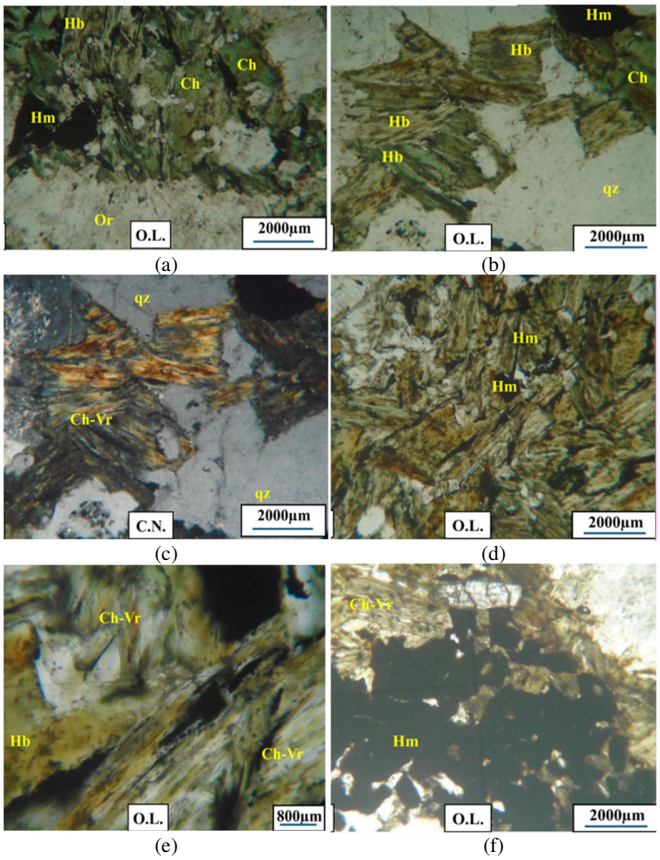

Fig. 12. Petrographic description of the hematitization of the chlorite and hornblende of the studied weathering profile in Al Barzah area: (a), (b), (c), (d): formation of parallel laminae of hematite and interstratified vermiculite, (e), (f): reddish-yellow and brown hematite flakes. Hb: hornblende, Ch: chlorite, Qz: quartz, Cl: clay minerals, Ch-vr: chlorite-vermiculite intergrade.

5) Quartz

Quartz occurs as angular to subrounded crystals in fresh parent granitic rocks. In the upper, highly weathered zone, quartz grains become highly fragmented and crushed. The resulting smaller quartz grains are usually stained by ferruginous clay materials. Highly corroded and embayed quartz grains are also observed, as shown in Figures 8 and 13(g-h).

III. CHEMICAL WEATHERING INDICES

The intensity and nature of the chemical weathering affecting the studied samples from the raw chemical data, were evaluated, as shown in Table I, using the Chemical Index of Alteration (CIA), the Chemical Index of Weathering (CIW), and the Plagioclase Index of Alteration (PIA). These indices are calculated from the molar proportions of major oxides, with CaO corrected for apatite contributions (CaO*). They are widely used in sedimentary, igneous, and metamorphic geochemistry to evaluate the intensity of silicate weathering, feldspar alteration, and element mobility during post-magmatic and surface processes.

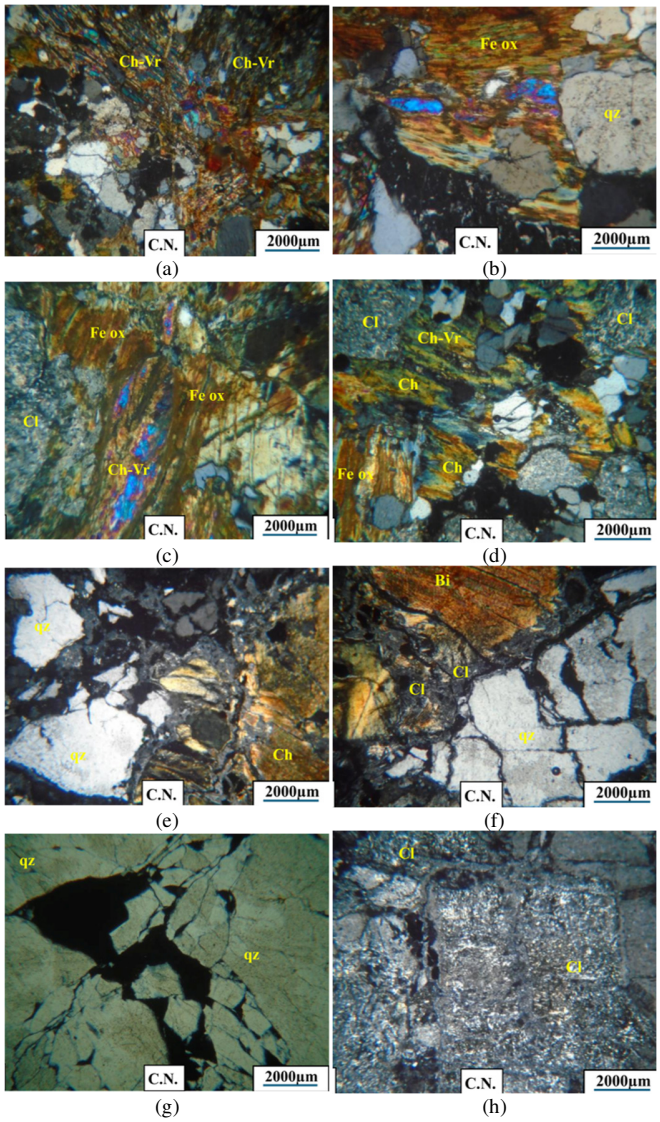

Fig. 13. (a), (b), (c), (d): Petrographic description of the hematitization of the chlorite and hornblende, (e), (f): hematitization of biotite; (g), (h): corrosion and embayment of the quartz by the enclosing kaolinitic matrix. Ch-Vr: chlorite-vermiculite intergrade, Qz: quartz, Cl: clay minerals, Fe-oxyhydroxides.

The CIA was calculated as:

$$CIA = 100 \times Al_2O_3 / (Al_2O_3 + CaO* + Na_2O + K_2O) \quad (1)$$

where CaO* is Ca incorporated in silicate minerals after correction for apatite using P_2O_5. The CIW, emphasizing the early-stage depletion of Ca and Na during plagioclase weathering, was calculated as [8]:

$$CIW = 100 \times Al_2O_3 / (Al_2O_3 + CaO* + Na_2O) \quad (2)$$

The PIA, reflecting the degree of plagioclase alteration relative to K-feldspar, was calculated as [9]:

$$PIA = 100 \times Al_2O_3 - K_2O / (Al_2O_3 + CaO* + Na_2O - K_2O) \quad (3)$$

A. Chemical Index of Alteration

The calculated CIA values for the studied samples, presented in Table II, show a wide range, from ~56 to ~89, indicating variable degrees of chemical weathering. Samples S1, S3, S4, S5, S6, S8, S10, and S11 have CIA values between ~56 and ~63, which is consistent with weak to moderate weathering and partial alteration of feldspar. These values are typical of relatively fresh to moderately altered feldspar-bearing igneous rocks. In contrast, samples S2 (CIA ≈ 84), S9 (CIA ≈ 79), and S12 (CIA ≈ 89) have higher CIA values, which reflect intense weathering and the leaching of mobile cations (Ca, Na, and K). These values are indicative of advanced weathering stages, which are typically associated with strong hydrolytic alteration, prolonged fluid-rock interaction, or residual aluminum enrichment during extreme chemical depletion [11].

TABLE I. CHEMICAL ANALYSES FOR THE STUDIED SAMPLES

Sample no.	**S1**	**S2**	**S3**	**S4**	**S5**	**S6**	**S7**	**S8**	**S9**	**S10**	**S11**	**S12**
SiO2	69.21	58.20	61.02	68.77	69.61	73	68.50	71.38	52.30	69.35	66.4	94.5
TiO2	0.33	0.80	0.29	0.35	0.35	0.2	0.35	0.22	1.10	0.53	0.49	0.15
Al2O3	14.48	24.50	14.47	14.87	14.74	14	18.20	14.06	18.50	14.2	15.8	2.50
Fe2O3	3.28	4.60	2.88	3.3	3.12	2.2	1.80	2.47	9.50	4.2	3.78	0.70
MnO	0.05	0.05	0.05	0.05	0.05	0.1	0.01	0.07	0.15	0.05	0.07	0.01
MgO	1.14	1.20	1.91	1.23	1.31	1	0.70	1.23	4.80	1.02	0.94	0.10
CaO	3.05	0.10	7.55	2.7	1.53	1.5	0.40	1.45	3.20	2.2	2.74	0.05
Na2O	3.94	0.20	1.72	3.92	4	2.3	1.50	2.4	1	4.42	3.45	0.01
K2O	2.23	1.80	1.72	2.52	2.58	3.7	4.80	3.53	1.50	2.23	5.78	0.30
P2O5	0.08	0.10	0.07	0.09	0.09	0	0.10	0.03	0.25	0.19	0.16	0.05
LOI	1.82	8.45	8.05	1.38	1.68	2.7	3.60	2.95	7.70	1.05	0.45	1.60
Total	99.61	100	99.73	99.18	99.06	100	99.96	99.79	100	99.44	100.06	99.96

TABLE II. CHEMICAL WEATHERING INDICES FOR THE STUDIED SAMPLES

Sample no.	**S3**	**S11**	**S1**	**S10**	**S4**	**S5**	**S6**	**S8**	**S7**	**S9**	**S12**	**S2**
Category	Parent rocks			Weathering profile								
Weathering intensity	W	WM	WM	WM	WM	WM	M	M	MS	SI	E	IE
CIA	44.57	49.77	50.92	53.12	52.34	55.49	57.04	57.90	70.1	70.9	88.4	91.5
CIW	47.28	61.99	55.65	58.39	57.90	62.14	68.47	68.71	87.5	75.6	99	98.7
PIA	43.87	49.63	51.11	53.80	52.90	56.98	60.57	61.53	83.5	73.9	99	98.6

W, weak alteration, MW, moderate to weak alteration,M, moderate alteration, MS, moderate to strong alteration, SI, strong to intensive alteration, E, extreme alteration, IE, intensive extreme alteration

B. Chemical Index of Weathering

The CIW values range from ~60 to nearly 100. Due to the exclusion of K_2O from the denominator, the CIW values systematically exceed the CIA values, thereby enhancing sensitivity to Ca and Na depletion. Samples S1, S3, S4, S5, S6, S8, S10, and S11 have CIW values ranging from ~65 to ~74, which indicates moderate plagioclase weathering and partial removal of Ca and Na. Exceptionally high CIW values are recorded in samples S2 (approximately 92), S9 (approximately 85), and S12 (approximately 99), which signifies near-complete depletion of Ca and Na, as well as advanced breakdown of plagioclase. These values suggest intense chemical alteration under conditions favoring strong leaching, such as prolonged exposure to meteoric fluids or acidic weathering environments. Sample S12 approaches the theoretical upper limit of CIW, which is consistent with extreme residual enrichment of Al.

C. Implications for Weathering Processes and Rock Evolution

The CIA–CIW–PIA values, suggest that the examined samples exhibit a wide range of chemical weathering intensities, from minimal alteration to severe chemical depletion. Most samples reflect feldspar-dominated protoliths affected by limited to moderate fluid-rock interaction, which is typical of relatively short weathering durations or semi-arid to temperate climatic conditions [10]. In contrast, samples S2, S9, and S12 are strongly weathered end-members, characterized by a significant loss of Ca, Na, and K relative to Al. Their geochemical signatures suggest prolonged surface weathering, intense hydrothermal alteration, or the residual concentration of Al-rich phases. On A–CN–K diagrams, as shown in Figure 14, these samples plot toward the Al apex, indicating advanced chemical maturation and a significant departure from primary igneous compositions [10].

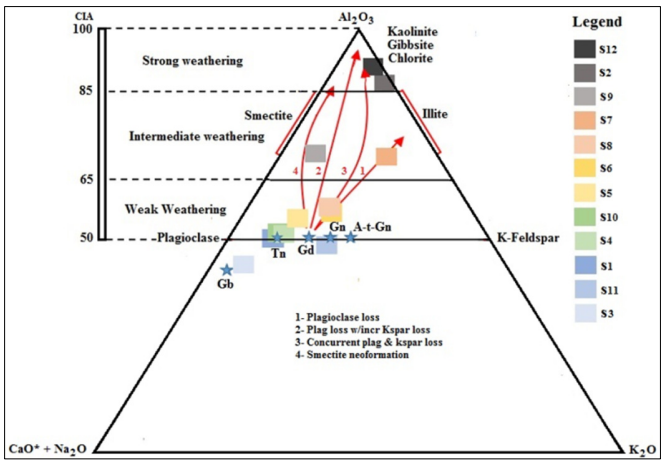

Fig. 14. CIA of the studied rocks. Gb: gabbro, Tn: tonalite, Gd: granodiorite, Gn: granite, A-t-Gn: alkali-type granite.

The revised weathering indices suggest:

- Chemical alteration ranges from weak to extreme among the studied samples.
- Plagioclase alteration is the dominant weathering process, particularly in highly altered samples.
- A subset of samples (S2, S9, and S12) shows intense chemical weathering and nearly complete feldspar breakdown.

Most samples, however, show moderate alteration patterns. On the A–CN–K ternary diagram, most samples are plotted along the feldspar weathering trend, which lies between the feldspar junction (CN–K) and the aluminum (Al) apex. This indicates a progressive depletion of calcium (Ca) and sodium (Na) relative to aluminum (Al). Samples S1, S3, S4, S5, S6, S8, S10, and S11 cluster near the feldspar compositional field. This is consistent with weak to moderate chemical weathering and incomplete feldspar alteration. In contrast, samples S2, S9, and S12 plot closer to the Al_2O_3 apex, reflecting advanced chemical maturation and intense leaching of mobile cations. Cross-plots of the CIA versus the CIW further emphasize this finding, with most samples falling within the low- to intermediate-weathering fields. However, S2, S9, and S12 define a distinct high-weathering population. A cross-plot of CIA versus CIW, as shown in Figure 15, highlights the full range of chemical weathering intensity. Samples S2, S9, and S12 occupy the high-weathering field, defining the advanced alteration endmember. This bimodality suggests variable alteration histories, likely reflecting differences in fluid availability, weathering duration, or localized hydrothermal overprinting.

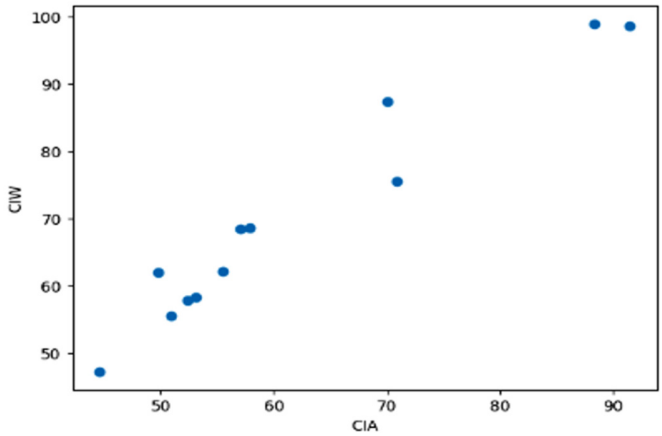

Fig. 15. CIA versus CIW cross-plot shows weathering intensity range of the studied samples.

IV. MASS-BALANCE WEATHERING ANALYSIS (T METHOD)

A. Basis of τ (Mass Transfer) Calculations

Mass-balance calculations were carried out using the classical approach, to quantify elemental gains and losses during chemical weathering [11]. The mass-transfer coefficient (τ) for element i was calculated relative to the immobile reference element (Al) according to:

$$\tau i = ((Ci/CAl)\ \text{sample} / (Ci/CAl)\ \text{parent}) - 1 \quad (4)$$

where Ci and CAl are the concentrations (wt.%) of element i Al_2O_3, respectively. Sample S3, which exhibits the lowest CIA, CIW, and PIA values, as well as minimal LOI, was selected as the least altered parent composition (fresh reference). Aluminum was treated as a stationary element during weathering, consistent with feldspar-dominated weathering systems and established geochemical practice.

B. Mass Transfer (τ) Results

Table III outlines the calculated τ values for CaO, Na_2O, and K_2O for all samples, with the results revealing a systematic redistribution of elements during progressive weathering:

- CaO and Na_2O exhibit strongly negative τ values ($\tau < -0.6$ to -0.99) in most samples, indicating the intense leaching of plagioclase-derived cations.
- K_2O exhibits variable behavior: positive τ values in moderately weathered samples reflect residual K-feldspar or secondary K enrichment, while negative τ values in highly weathered samples (S2, S9) indicate late-stage K loss.
- SiO_2 shows depletion or enrichment depending on weathering intensity, reflecting quartz stability and residual concentration in strongly weathered profiles. These patterns are diagnostic of progressive feldspar breakdown and aluminum-residual enrichment, consistent with classical silicate weathering trajectories [12].

TABLE III. MASS TRANSFER RESULTS RELATIVE TO IMMOBILE AL (PARENT = S3)

Sample	τ (CaO)	τ (Na_2O)	τ (K_2O)
S3 (parent)	0.00	0.0	0.0
S1	-0.60	+1.29	+0.30
S2	-0.99	-0.95	-0.39
S4	-0.65	+1.26	+0.43
S5	-0.80	+1.30	+0.47
S6	-0.79	+0.38	+1.22
S7	-0.96	-0.31	+1.12
S8	-0.80	+0.43	+1.24
S9	-0.67	-0.55	-0.31
S10	-0.70	+1.61	+0.45
S11	-0.67	+0.84	+2.07
S12	-0.99	-0.97	-0.30

The τ values were calculated using sample S3 as the least altered parent. CaO and Na_2O exhibit strongly negative τ values in most samples, indicating substantial leaching. In contrast, K_2O shows variable τ behavior, reflecting intermediate enrichment and late-stage depletion. Plotting the τ values against the relative weathering position, as presented in Figure 16, reveals an early, rapid loss of Ca and Na, a transitional redistribution of K, and a near-complete depletion of the mobile alkalis in the most intensely weathered samples.

C. Vertical Chemical Gradients Through the Profile

Figure 17 shows the vertical variation of major oxides. Samples are arranged according to increasing CIA (a proxy for profile position). The plots show:

- Systematic depletion of CaO and Na_2O with increasing weathering.
- Relative enrichment of Al_2O_3 and variable K_2O behavior, consistent with progressive feldspar breakdown.

This vertical variation is reflected in the τ plots, which demonstrate negative values of Ca and Na with increasing weathering, confirming that open-system behavior results from downward leaching.

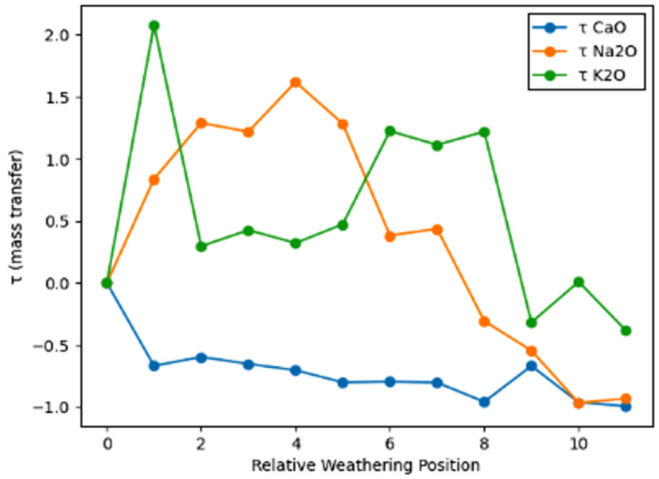

Fig. 16. τ (mass transfer) trend versus weathering profile position.

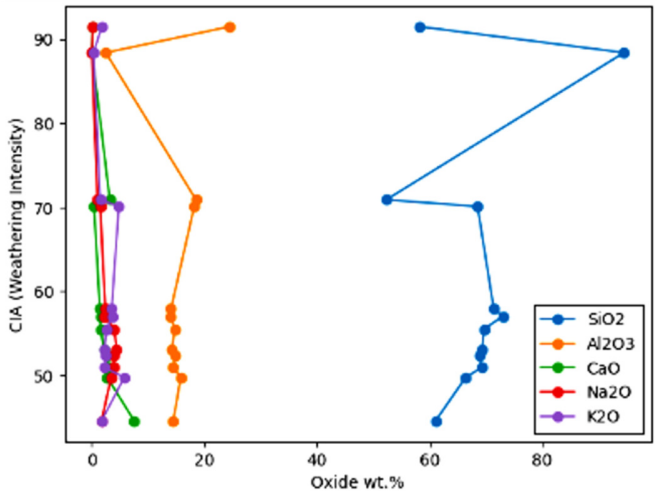

Fig. 17. Vertical variation of major oxides.

D. τ Plots Interpretation

The τ plots ($CaO–Na_2O–K_2O$ versus profile position) reveal:

- Early-stage weathering, which is characterized by rapid loss of Ca and Na (negative τ) and minor K redistribution.
- Intermediate stage, which is characterized by partial K enrichment due to residual concentration or secondary K-bearing phases.
- Advanced weathering, which is characterized by near-complete depletion of Ca, Na, and K, producing Al-rich residual compositions.

Negative τ values indicate elemental loss, while positive values indicate relative enrichment. This evolution matches the A–CN–K weathering trend and quantitatively validates the CIA–CIW–PIA interpretations.

V. CONCLUSIONS

The weathering of the Al Barzah granites occurred in two stages: transformation and neoformation. These processes progressively destroyed the original crystalline texture of the parental granitic rocks and altered the feldspars, hornblende, biotite, and quartz. This resulted in the formation of sericite and kaolinite in place of the feldspars during the initial and mid stages of alteration, ultimately yielding kaolinitic clays. Mafic minerals undergo progressive alteration during initial transformation, forming iron oxides along their cleavage planes, and finally forming mixed clays, goethite, and hematite minerals. Authors in [13] concluded that the mineral assemblage is usually subdivided into five zones from top to bottom: the completely weathered zone, the highly weathered zone, the moderately weathered zone, the slightly weathered zone, and the fresh rock mass. Authors in [14, 15] showed that the mineral transformations in different weathering stages exhibit the following sequences of mineral alteration: feldspar – sericite – hydromica - kaolinite, pyroxene – hornblende - chlorite-montmorillonite – halloysite - kaolinite, biotite – vermiculite – montmorillonite - kaolinite, and quartz – silica – chalcedony - secondary quartz. Conversely, authors in [16] pointed out that the chemical weathering of common rock-forming minerals produces only a few abundant groups of secondary minerals, while authors in [17] defined five weathering classes according to the macroscopic appearance of hand specimens, grain sizes, friability, and color determination in weathering profiles in SW Bornholm. The transformation and replacement of parental minerals and the destruction of the original crystalline texture demonstrate the importance of weathering processes under humid tropical conditions. These conditions existed during the exposure of granitic rocks before the deposition of the well-pronounced tertiary unconformity surface.

REFERENCES

[1] A. M. Al-Shanti, *Oolitic Iron Ore Deposits in Wadi Fatima: Between Jeddah and Mecca, Saudi Arabia*. Jeddah, Saudi Arabia: Ministry of Petroleum and Mineral Resources, 1966.

[2] T. A. Moore and M. H. Al-Rehaili, *Expanatory Notes to the Geologic Map of the Makkah Quadrangle, Sheet 21D, Kingdom of Saudi Arabia*. Jeddah, Saudi Arabia: Ministry of Petroleum and Mineral Resources, Directorate General of Mineral Resources, 1989.

[3] P. R. Johnson, *Explanatory Notes to the Map of Proterozoic Geology of Western Saudi Arabia*, Technical Report SGS-TR-2006-4, Jeddah, Kingdom of Saudi Arabia: Saudi Geological Survey, 2006.

[4] A. A. Mesaed, M. Gameil, and R. F. Thiga, "Stratigraphic Setting, Facies Types, and Mineral Paragenesis of the Carbonate-Bearing Tertiary Sedimentary Succession of Usfan Area, West-Central Saudi

Arabia," *Engineering, Technology & Applied Science Research*, vol. 15, no. 6, pp. 28818–28828, Dec. 2025, https://doi.org/10.48084/etasr.13394.

[5] Y. Tardy, "Geochemistry of weathering: a study of the sands and waters of some crystalline massifs in Europe and Africa," M.S. thesis, University of Strasbourg, Strasbourg, France, 1971.

[6] A. A. Mesaed, "Weathering of Precambrian chlorite schist and formation of Fe-laterite, Quseir–Qift Road, Eastern Desert, Egypt," in *Proceedings of the 5th International Conference on Geology of the Arab World*, vol. 1, pp. 390–393, 2000.

[7] H. W. Nesbitt and G. M. Young, "Early Proterozoic climates and plate motions inferred from major element chemistry of lutites," *Nature*, vol. 299, pp. 715–717, 1982, https://doi.org/10.1038/299715a0.

[8] L. Harnois, "The CIW index: A new chemical index of weathering," *Sedimentary Geology*, vol. 55, nos. 3–4, pp. 319–322, 1988, https://doi.org/10.1016/0037-0738(88)90137-6.

[9] C. M. Fedo, H. W. Nesbitt, and G. M. Young, "Unraveling the effects of potassium metasomatism in sedimentary rocks and paleosols, with implications for paleoweathering conditions and provenance," *Geology*, vol. 23, pp. 921–924, 1995, https://doi.org/10.1130/0091-7613(1995)023<0921:UTEOPM>2.3.CO;2.

[10] S. M. McLennan, S. Hemming, D. K. McDaniel, and G. N. Hanson, "Geochemical approaches to sedimentation, provenance, and tectonics," in *Processes Controlling the Composition of Clastic Sediments*, *Geological Society of America Special Paper*, vol. 284, pp. 21–40, 1993, https://doi.org/10.1130/SPE284-p21.

[11] H. W. Nesbitt and G. M. Young, "Prediction of some weathering trends of plutonic and volcanic rocks based on thermodynamic and kinetic considerations," *Geochimica et Cosmochimica Acta*, vol. 48, no. 7, pp. 1523–1534, 1984, https://doi.org/10.1016/0016-7037(84)90408-3.

[12] M. Sundararajan, B. Nallusamy, M. V. Sonisha, M. A. Pasha, and M. A. M. Aslam, "Geochemistry of the core sediments of Thiruchendur Coast, Tamil Nadu, India," in *Geochemistry and Mineralogy of Coastal Sediments in Tamil Nadu*, M. Sundararajan, B. Nallusamy, M. A. Mohammed Aslam, and S. Chidambaram, Eds., pp. 1–21, India: Aarhat Publication & Aarhat Journals, 2017.

[13] Z. G. Huang, W. Q. Chen, and J. H. Chen, *Red Weathered Crust in South China*, Beijing, China: Chinese Ocean Press, 1996.

[14] Y. L. Wang, "Micro-Study on Bedrock Weathering Crust of Three Gorges and its Classification," in *Proceedings of the Fourth Conference of Engineering Geology*, 1992.

[15] F. L. Li, "Distribution characters and grade classification of weathering rocks in the area along the coast of China," *Harbor Reconnaissance*, vol. 3, pp. 9–14, 1987.

[16] H. W. Nesbitt and G. M. Young, "Formation and diagenesis of weathering profiles," *The Journal of Geology*, vol. 97, no. 2, pp. 129–147, 1989, https://doi.org/10.1086/629290.

[17] C. Ollier and C. Pain, *Regolith, Soils and Landforms*, Chichester, UK: John Wiley & Sons, 1996.